Supporting information

Hydrogen Evolution Reaction Boosted by Bridge Bonds between Electrocatalyst and Electrode

Guanglei Liu,[†, ‡, ∇] Zhanyu Wang,[#, ∇] Lianhai Zu,[†, ‡] Yan Zhang,[†] Yutong Feng,[†] Shihe Yang,[§] Yu Jia,[¶] Songyou Wang,[#] Chi Zhang[†] and Jinhu Yang*[, †, ‡]

[†]School of Chemical Science and Engineering, Tongji University, Siping Road 1239, Shanghai 200092, P. R. China

[‡]Research Center for Translational Medicine & Key Laboratory of Arrhythmias of the Ministry of Education of China, East Hospital, Tongji University School of Medicine, No. 150 Jimo Road, Shanghai 200120, P. R. China

[#]Shanghai Ultra-Precision Optical Manufacturing Engineering Center and Department of Optical Science and Engineering, Fudan University, Shanghai 200433, P. R. China

[§]Department of Chemistry, the Hong Kong University of Science and Technology, Clear Water Bay, Kowloon, Hong Kong, P. R. China

[¶]Key Laboratory for Special Functional Material of Ministry of Education, and School of Physics and Electronics, Henan University, Kaifeng 475001, P. R. China

Experimental Section

Preparation of $Co(OH)_3$ nanobelts grown on Ti foil ($Co(OH)_3$ nanobelts/Ti). The synthesis of $Co(OH)_3$ nanobelts/Ti was carried out referring to our previously reported method[1] with some modifications. Firstly, 0.0055 g of $CoCl_2 \cdot 6H_2O$ was dissolved into 5 ml H_2O and 0.012 g of CTAC (hexadecyltrimethyl-ammonium chloride) was dissolved into 5 ml DMF, respectively. Then the two solutions were mixed and transferred into a 50 ml Teflon-lined stainless autoclave, followed by the dropwise addition of 2 ml H_2O_2 (30 wt%), giving a transparent pink solution. Afterwards, a piece of bare Ti foil was immersed into the mixed solution, and the autoclave was sealed and kept at 150 °C for 20 hours. Finally, after the reaction system was cooled down in air, the Ti foil grown with $Co(OH)_3$ nanobelts was taken out, rinsed separately with water and absolute ethanol, and dried at 80 °C for several hours. For comparison, $Co(OH)_3$ nanobelts formed in solution ($Co(OH)_3$ nanobelts (aq.)) were also collected by centrifugation at 5000 rpm for 5 min, and washed with deionized water and absolute ethanol.

Preparation of CoS_2 nanobelts assembled on Ti foil (CoS_2 nanobelts/Ti). CoS_2 nanobelts/Ti was obtained through a two-step *in situ* chemical transformation of $Co(OH)_3$ nanobelts in a horizontal quartz tube furnace. Firstly, $Co(OH)_3$ nanobelts/Ti was calcined at 300 °C for 2 h in air, leading to the formation of morphology-preserved Co_3O_4 nanobelts on Ti foil (Co_3O_4 nanobelts/Ti). Then, Co_3O_4 nanobelts/Ti was placed in middle of the tube furnace, and 2 g of sulfur powder was placed at the upstream side. The tube was flushed with Ar several times to drive redundant air

51 away, and then maintained under a steady Ar flow at a speed of 25 sccm during the
52 sulfidation procedure at 400 °C. After 6 h, the sample was cooled down naturally to
53 room temperature and rinsed successively with CS_2 and absolute ethanol. The average
54 mass loading of CoS_2 samples on Ti foil was ~0.667 mg cm^{-2}, calculated according to
55 the mass difference between Ti foil and the CoS_2 nanobelts/Ti. For comparison,
56 $Co(OH)_3$ nanobelts (aq.) were also placed on a Ti foil and *in situ* converted to CoS_2
57 nanobelts (CoS_2 nanobelts(aq.)) through the same procedure.

58 **Characterization.** Morphology was characterized by using a scanning electron
59 microscope (SEM, Hitachi S4800, 3 kV) equipped with an associated energy-
60 dispersive X-ray spectroscopy (EDX) and a high-resolution transmission electron
61 microscope (HR-TEM, JEM 2011, 200 kV). The crystal structure was determined by
62 X-ray diffraction (XRD) using a D/max2550VB3+/PC X-ray diffractometer with Cu
63 Kα radiation with a 1.5418 °A wavelength. A beam voltage of 40 kV and a 100 mA
64 current beam were used. Raman spectrum was recorded by using a spectrophotometer
65 (inVia, Renishaw, Germany) with a 514 nm laser. The relative electronic states were
66 investigated by X-ray photoelectron spectroscopy (XPS) in a PHI-5000C ESCA
67 system (Perkin-Elmer) with Mg Kα radiation. All binding energies (BEs) were
68 referred to the C 1s peak (284.6 eV) arising from surface hydrocarbons (or
69 adventitious hydrocarbons).

70 **Electrochemical measurements.** All the electrochemical measurements were
71 conducted with the standard three-electrode setup in an electrochemical cell by using
72 a CHI660E electrochemical workstation (CH Instruments, Inc., Shanghai) at ambient

temperature. The sample (CoS_2 nanobelts/Ti) was directly used as a binder-free working electrode, a graphite rod as the counter electrode and a saturated calomel electrode (SCE) as the reference electrode. For comparison, Co_3O_4 nanobelts/Ti, CoS_2 nanobelts (aq.) as well as Ti foil and Pt wire were also investigated as working electrodes. CoS_2 nanobelts (aq.) were immobilized on a Ti foil (CoS_2 nanobelts (aq.)-Ti) using Nafion diluent solution as the adhesive agent, with a mass loading of 0.667 mg cm^{-2} that is the same as the CoS_2 nanobelts/Ti. Prior to the electrochemical test, the electrolyte solution was bubbled with high-purity N_2 (≥99.99%) for 10 min to eliminate the dissolved oxygen. Linear sweep voltammetry (LSV) measurements were conducted in 0.5 M H_2SO_4 solution with a scan rate of 2 $mV \cdot s^{-1}$. Electrochemical impedance measurements (EIS) were carried out with an amplitude of 5 mV in the frequency range from 100 kHz to 0.01 Hz. The hydrogen generation stability of CoS_2 nanobelts/Ti was carried out by using amperometric I-t curves with a period of 20 hours at a constant potential. Besides 0.5 M H_2SO_4 solution, the electrochemical measurements were conducted in 1.0 M disodium hydrogen phosphate buffer solution (PBS) (neutral environment) and 1.0 M KOH solution (basic environment) in the same configuration. All polarization curves were corrected with I-R compensation by relevant impedance measurements. Potentials were referenced to the reversible hydrogen electrode (RHE) by adding a value of (0.242 + 0.059 pH) V.

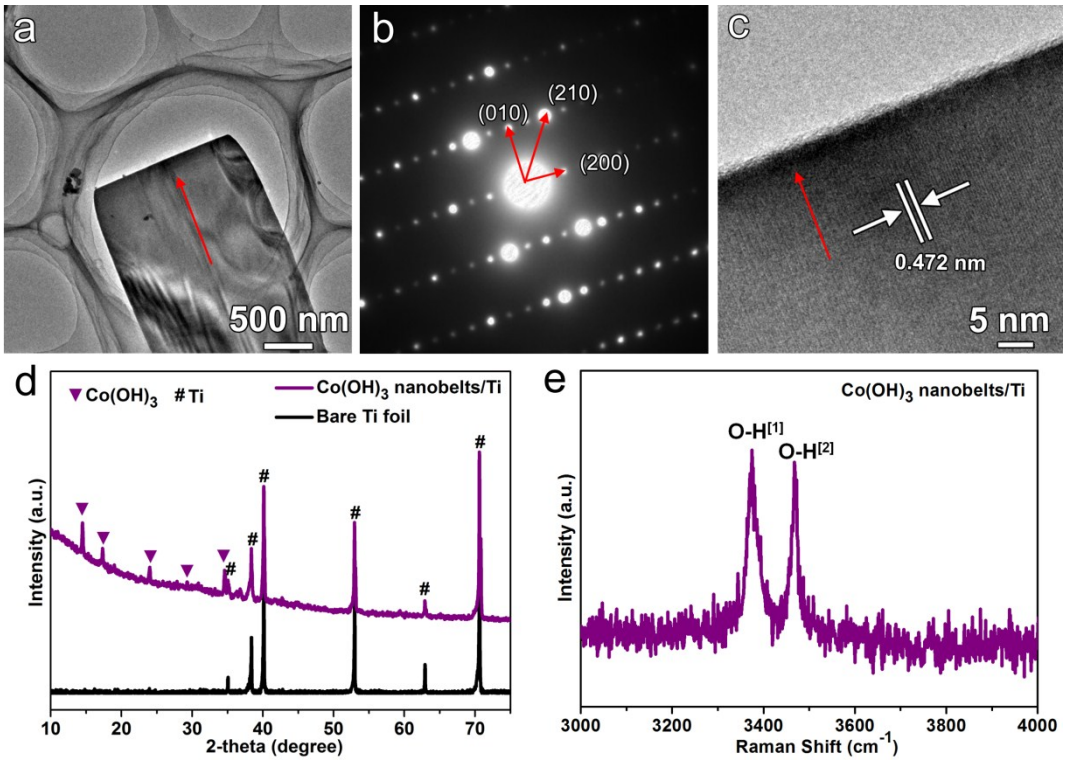

Figure S1. TEM images (a, c), selected-area electron diffraction pattern (b), XRD pattern (d), Raman spectrum (e) of the typical $Co(OH)_3$ nanobelts/Ti.

The $Co(OH)_3$ nanobelts exfoliated from the Ti foil were characterized by TEM in Figures S1a-S1c. As shown in Figure S1a, a single nanobelt presents rectangular edges and uniform thickness, in accordance with the SEM characterization in Figures 2a and 2b. The ordered electron diffraction (ED) pattern (Figure S1b) and continuous crystal lattice lines (Figure S1c) indicate a single crystal structure of the nanobelt with the exposed surface of (001) planes and the growth direction of [010].[1] The XRD pattern of the $Co(OH)_3$ nanobelts/Ti exhibits a set of diffraction peaks indexed well to monoclinic structured $Co(OH)_3$,[1] in addition to the peaks from the Ti substrate. Raman spectrum of nanobelts shows two distinct peaks at 3374 cm^{-1} ($O\text{-}H^{[1]}$) and 3467 cm^{-1} ($O\text{-}H^{[2]}$), which belong to the vibrations of O-H groups from intermolecular interaction and inside crystals,[1] respectively.

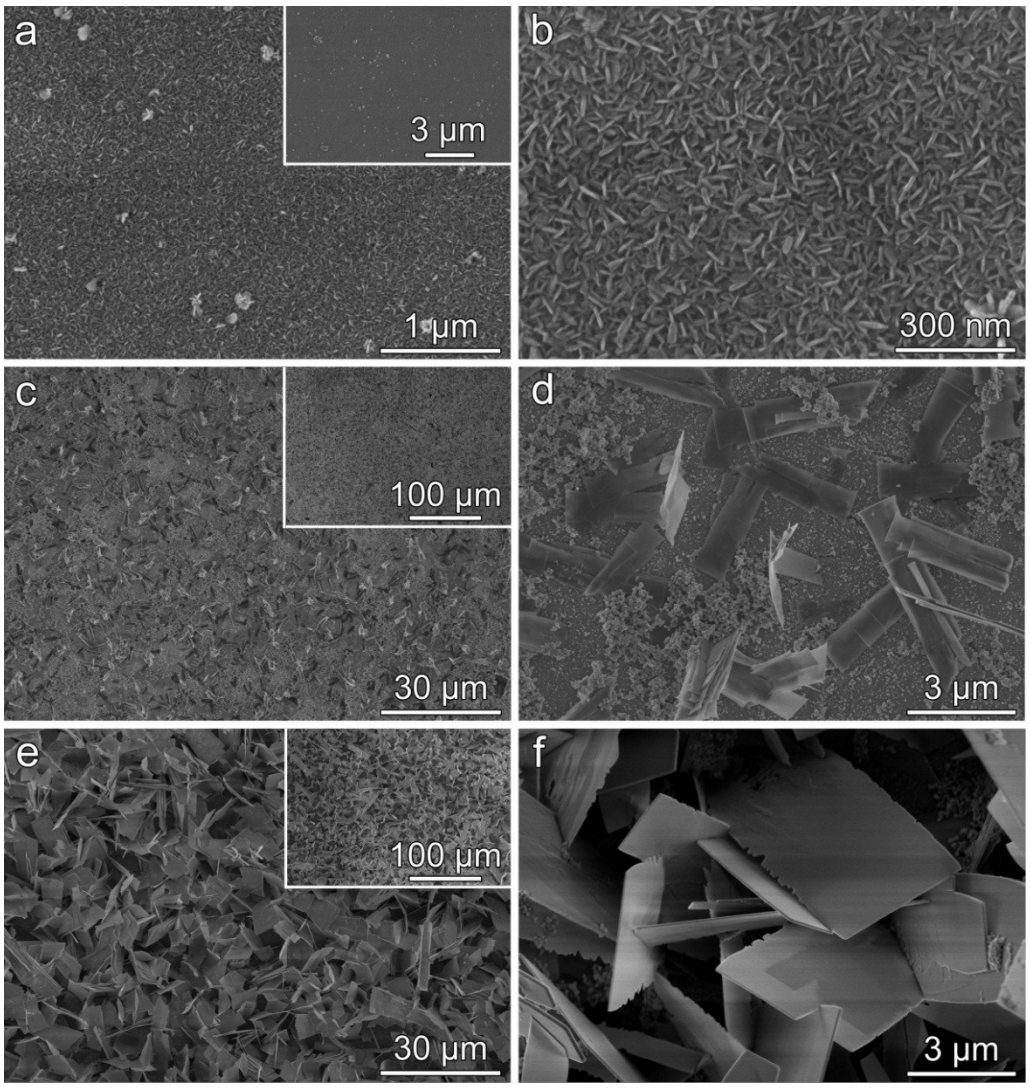

Figure S2. SEM images of $Co(OH)_3$ nanobelts/Ti samples obtained at different reaction times of 1 h (a, b), 5 h (c, d) and 10 h (e, f). Insets in (a, c, e) are the corresponding low-magnification images.

As shown in Figures S2a and S2b, the branch-like samples are densely assembled on Ti foil at 1 h, with a tiny size of ~10 nm in diameter and ~50 nm in length, respectively. When the time is increased to 5 h, the branches grow up to small nanobelts (Figures S2c and S2d) and bond tightly to the Ti foil, holding a size of ~1 μm in width and ~3 μm in length, respectively, with some Co_3O_4 particles of ~100 nm in diameter depositing on the substrate from solution. At 10 h, the large nanobelts are formed, which are nearly identical in size and morphology to the typical samples with the growth time of 20 h (Figures 2a and 2b in the main text).

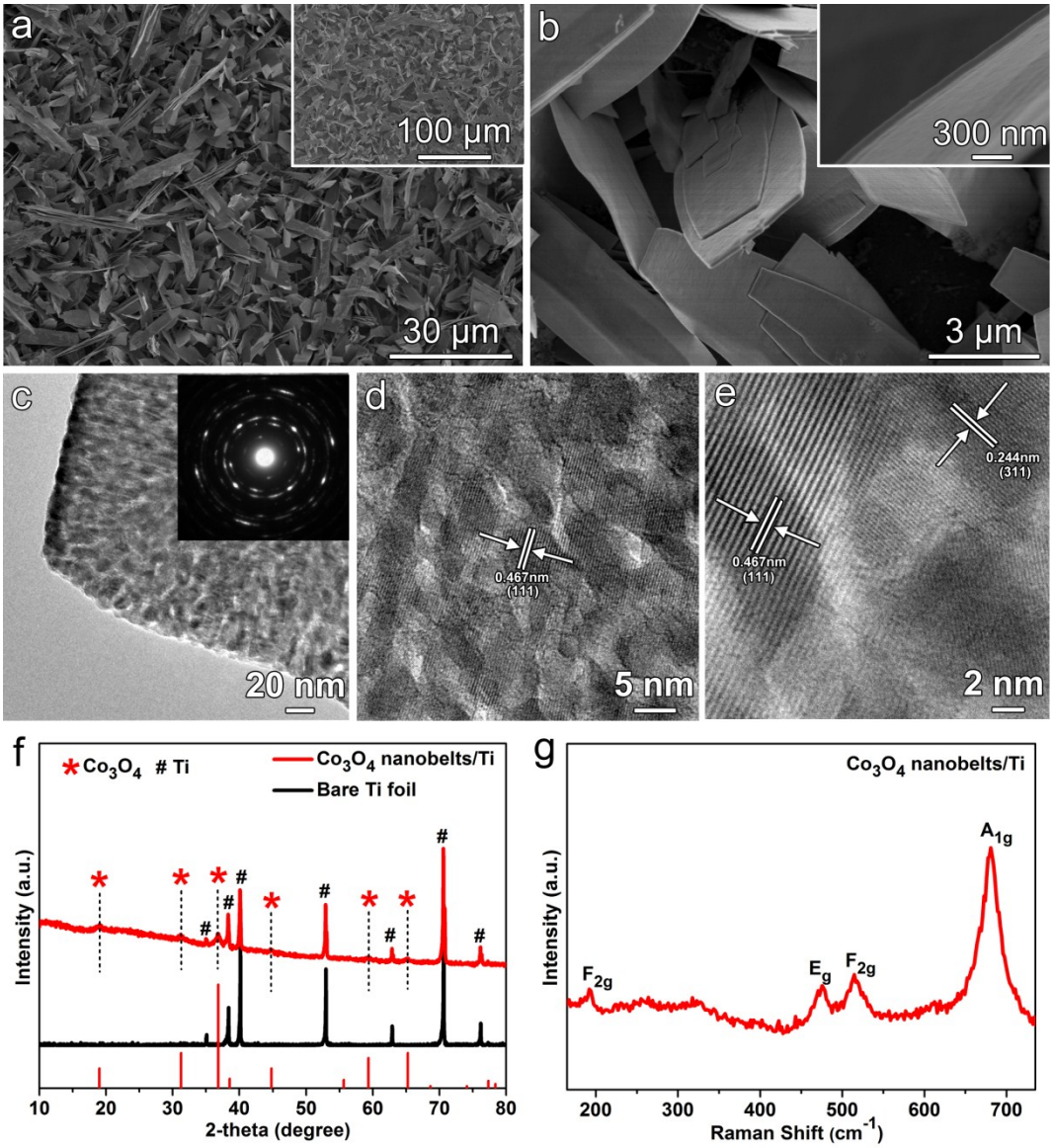

Figure S3. SEM images (a, b), TEM images (c-e), XRD pattern (f) and Raman spectrum (g) of the Co_3O_4 nanobelts/Ti. Inset in (c) is the corresponding selected area electron diffraction pattern.

It can be seen from Figures S3a and S3b that the morphology between $Co(OH)_3$ and Co_3O_4 nanobelts has no obvious difference. However, the surface of Co_3O_4 nanobelts become rougher compared with $Co(OH)_3$ nanobelts from the inset of Figure S3b. TEM images with selected area electron diffraction (SAED) indicate that Co_3O_4 nanobelts consist of numerous crystalline grains, accompanying with the crystal structure changing from a single crystal ($Co(OH)_3$) to a pseudo-single crystal (the

inset of Figure S3c). The lattice fringes with d values of 0.467 and 0.244 nm can be assigned to the diffractions planes of (200) and (211), corresponding to Co_3O_4 (Figures S3d and S3e). All diffraction peaks of the XRD pattern are well matched with cubic crystal Co_3O_4 (JCPDS No. 42–1467) and Ti (JCPDS No.89–4893) (Figure S3f). The Raman spectrum of Co_3O_4 nanobelts shows several typical peaks at 192, 476, 515, 680 cm^{-1}, corresponding to F_{2g}, E_g, F_{2g}, A_{1g},[2] respectively, further proving a pure phase of Co_3O_4.

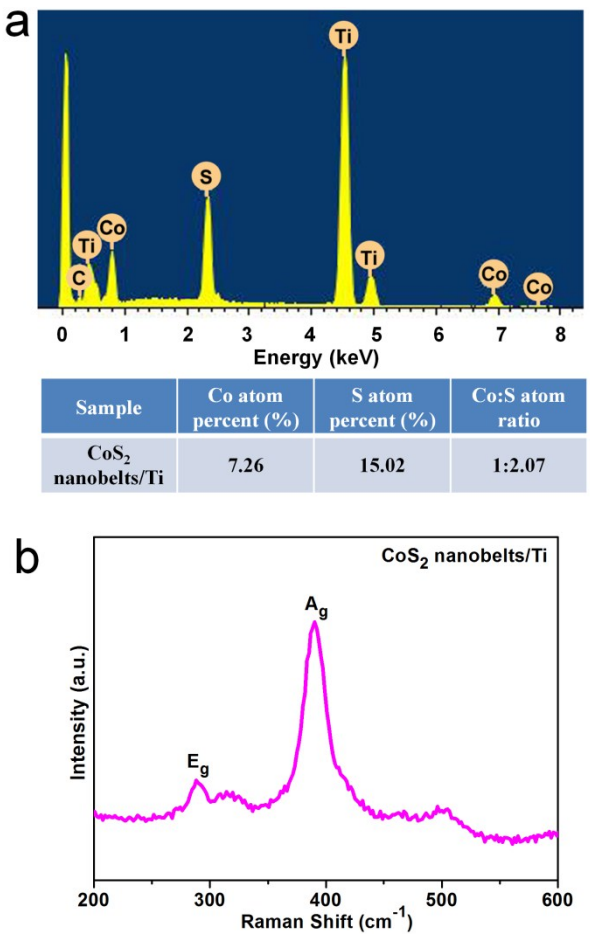

Sample	Co atom percent (%)	S atom percent (%)	Co:S atom ratio
CoS_2 nanobelts/Ti	7.26	15.02	1:2.07

Figure S4. EDS (a) and Raman spectrum (b) of the CoS_2 nanobelts/Ti.

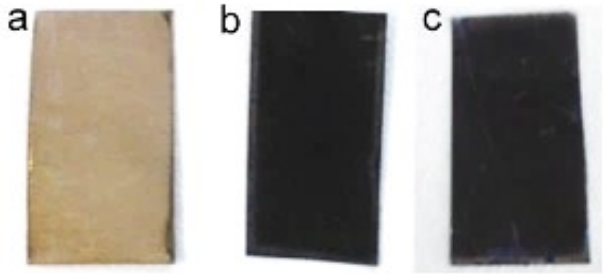

Figure S5. Optical photographs of the $Co(OH)_3$ nanobelts/Ti (a), the Co_3O_4 nanobelts/Ti (b) and the CoS_2 nanobelts/Ti (c).

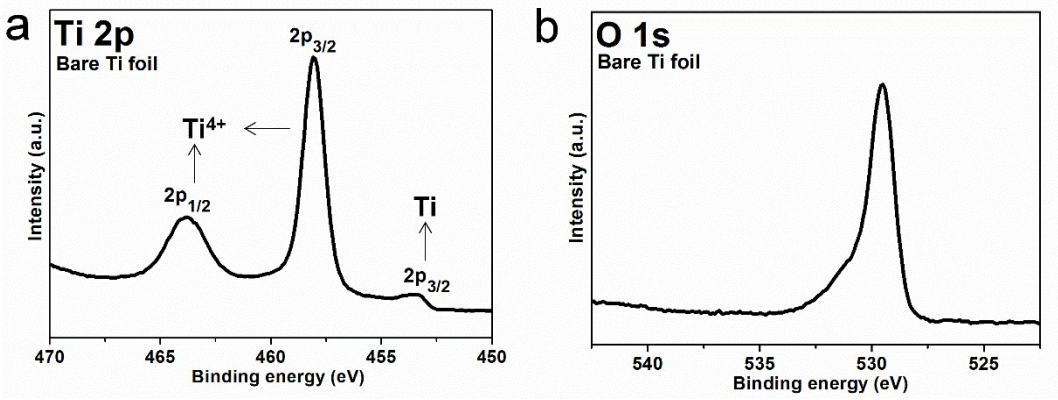

Figure S6. XPS spectra of Ti 2p and O 1s for bare Ti foil.

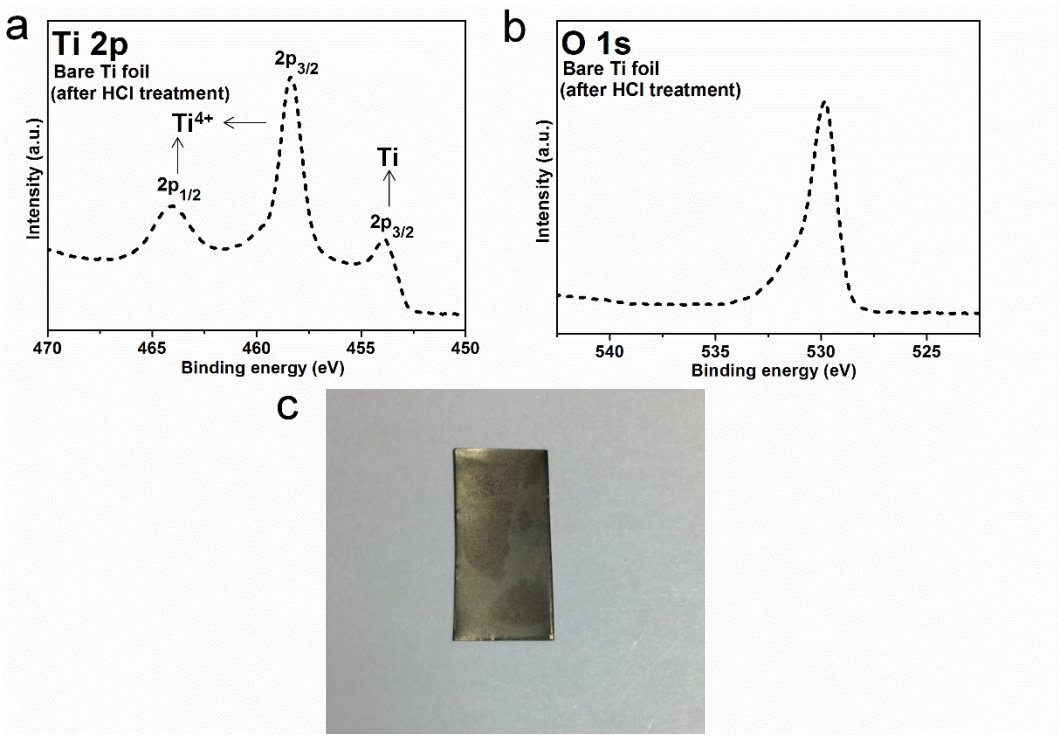

Figure S7. (a, b) XPS spectra of Ti 2p (a) and O 1s (b) for bare Ti foil after the ultrasound bath treatment in concentrated HCl solution for 30 min. (c) Optical photograph of the $Co(OH)_3$ nanobelts *in situ* grown on the Ti foil which beforehand underwent concentrated HCl solution treatment.

For comparison, we investigated the Ti foil which is cleaned by the ultrasound bath treatment in concentrated HCl solution for 30 min. As is shown in Figure S7a, the XPS data of Ti 2p from the bare Ti foil after HCl treatment exhibits three arrowed typical peaks, containing two strong peaks corresponding to Ti $2p_{1/2}$ and $2p_{3/2}$ for Ti^{4+} (TiO_2) and a weak peak corresponding to Ti $2p_{3/2}$ for Ti (metal Ti), respectively. The XPS spectrum of O in Figure S7b shows the typical peak of O 1s for O^{2-} (TiO_2). Specifically, for the Ti foil after HCl treatment, the thin TiO_2 layer on surface still exists which is actually very difficult to be eliminated by concentrated HCl solution, while the peak of Ti $2p_{3/2}$ for metal Ti (Figure S7a) becomes evidently higher compared with the counterpart from the Ti foil without HCl treatment (Figure S6a). Meanwhile, Table S1 shows relevant surface atomic concentration for both kinds of

Ti foil based on XPS data, and we find the concentrated HCl solution treatment makes the ratio of Ti:O increase from 1:2.882 to 1:1.886 on Ti foil surface, indicating the decrement of O content and the increase of Ti content on the surface of the Ti foil. The optical photograph in Figure S7c shows the $Co(OH)_3$ nanobelts were only grown on parts of surface of the Ti foil after HCl treatment under the same hydrothermal synthesis in Experimental Section of Supporting Information. We think HCl treatment may destroy some TiO_2 layer, which makes a few metal Ti atoms exposed on the surface of Ti foil, preventing the *in situ* growth of $Co(OH)_3$ nanobelts (Figure S7c). Accordingly, we speculate the thin oxide layer may serve as an effective adhering layer for *in situ* nucleation, growth and subsequent assembly of $Co(OH)_3$ nanobelts (Figure 2a) on the substrate.

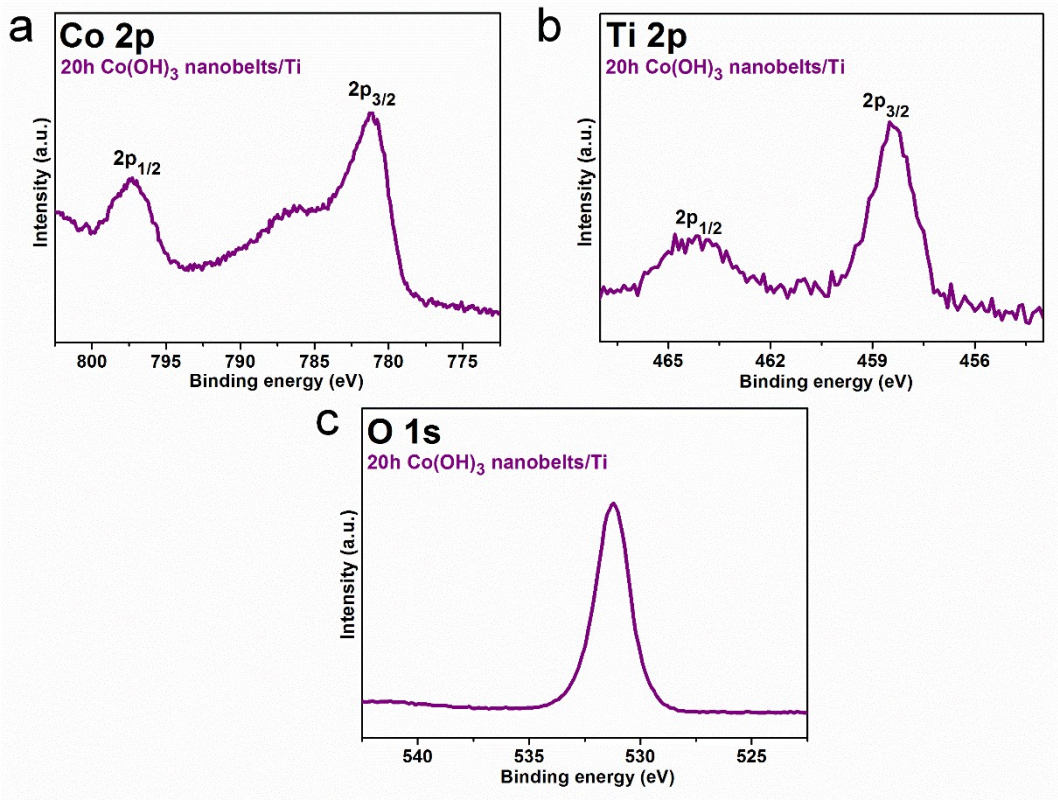

Figure S8. XPS spectra of Co 2p, Ti 2p and O 1s for the typical $Co(OH)_3$ nanobelts/Ti

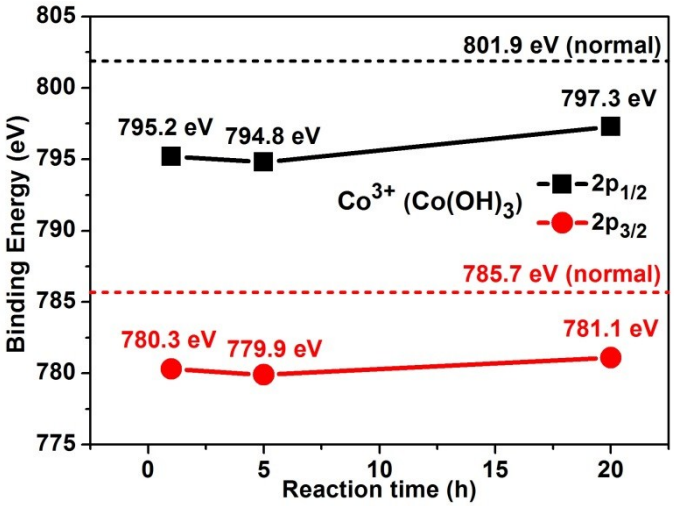

Figure S9. Schematic diagram shows XPS binding energy of Co 2p for $Co(OH)_3$ nanobelts/Ti samples obtained at different growth times of 1 h, 5h and 20 h, respectively.

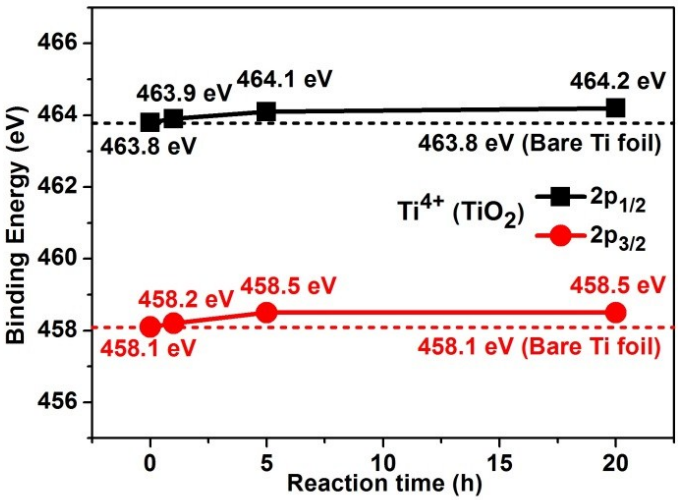

Figure S10. Schematic diagram shows XPS binding energy of Ti 2p for $Co(OH)_3$ nanobelts/Ti samples obtained at different growth times of 0 h, 1 h, 5 h and 20 h, respectively.

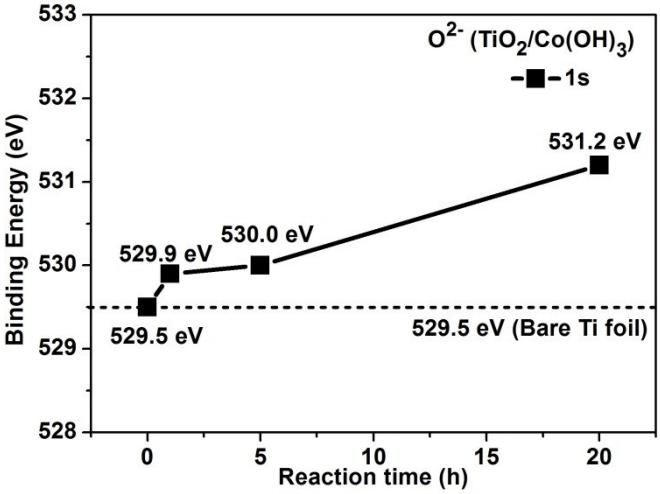

Figure S11. Schematic diagram shows XPS binding energy of O 1s for $Co(OH)_3$ nanobelts/Ti samples obtained at different growth times of 0 h, 1 h, 5h and 20 h, respectively.

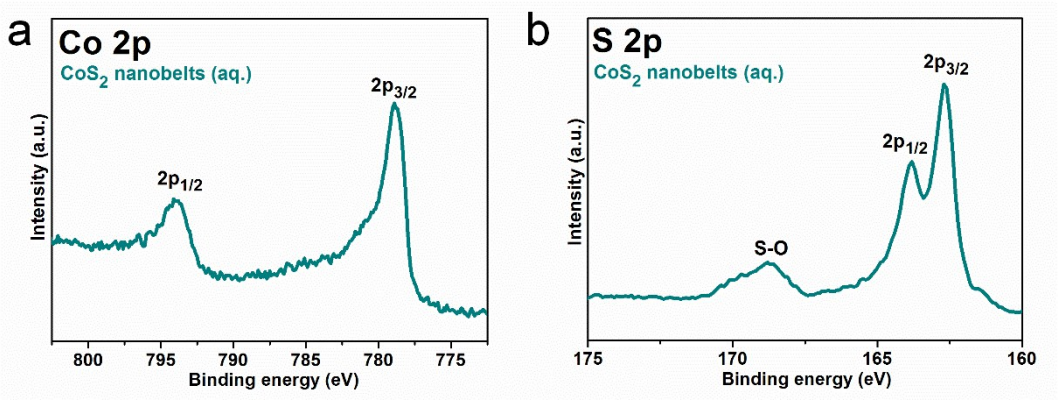

Figure S12. XPS spectra of Co 2p and S 2p for the CoS_2 nanobelts (aq.).

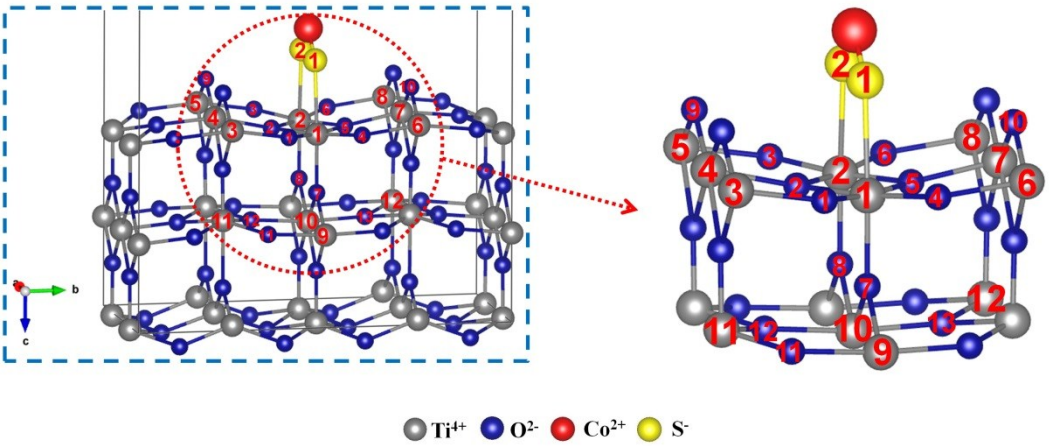

Figure S13. Schematic view of DFT simulation for Ti-S and Ti-O bonds from CoS_2 nanobelts/Ti.

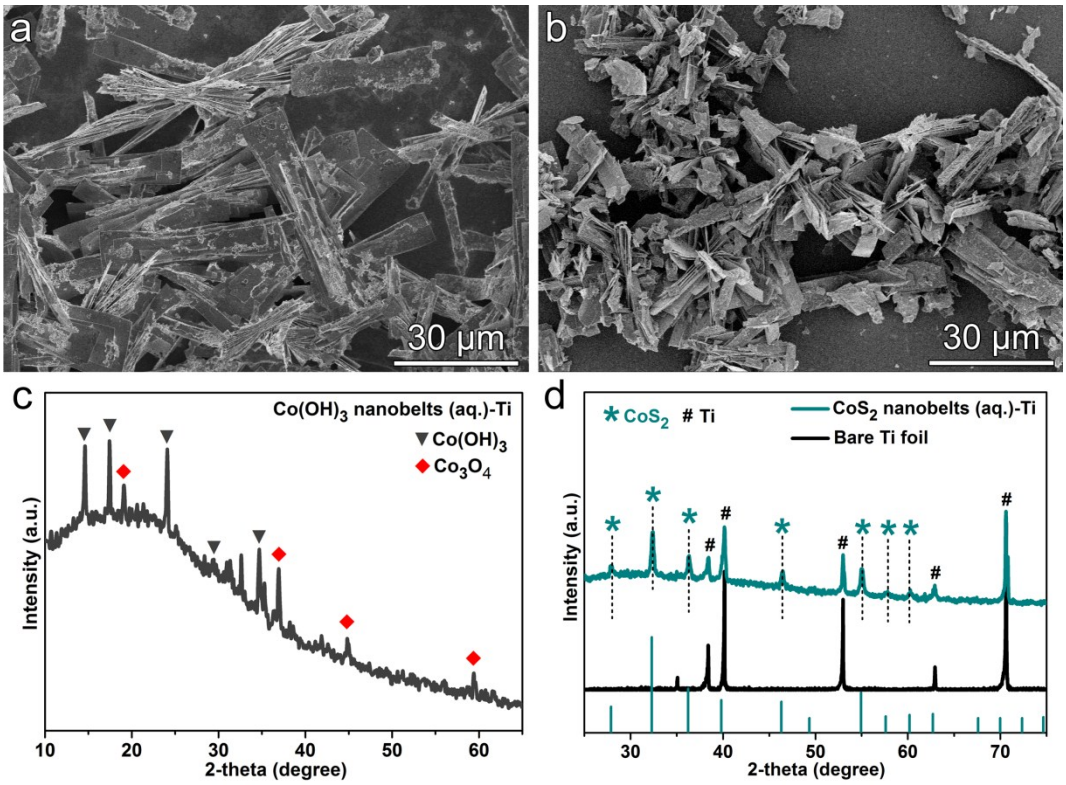

Figure S14. SEM images (a, b) and XRD patterns of (c, d) for $Co(OH)_3$ nanobelts (aq.) (a, c) from solution, and CoS_2 nanobelts (aq.)-Ti (b, d) obtained from transformation of the $Co(OH)_3$ nanobelts (aq.).

The precursor $Co(OH)_3$ nanobelts (aq.) are almost the same as the typical $Co(OH)_3$ nanobelts/Ti in shape, with some Co_3O_4 particles deposited on their surfaces (Figure S14a). The relevant diffraction peaks of the corresponding XRD pattern match well with the monoclinic structured $Co(OH)_3$ accompanying with several Co_3O_4 diffraction peaks from the particles (Figure S14c). After the same thermal conversion and sulfidation procedure, CoS_2 nanobelts (aq.) were prepared (Figure S14b) and proved to be pure-phase CoS_2 by XRD (JCPDS No. 41–1471) (Figure S14d).

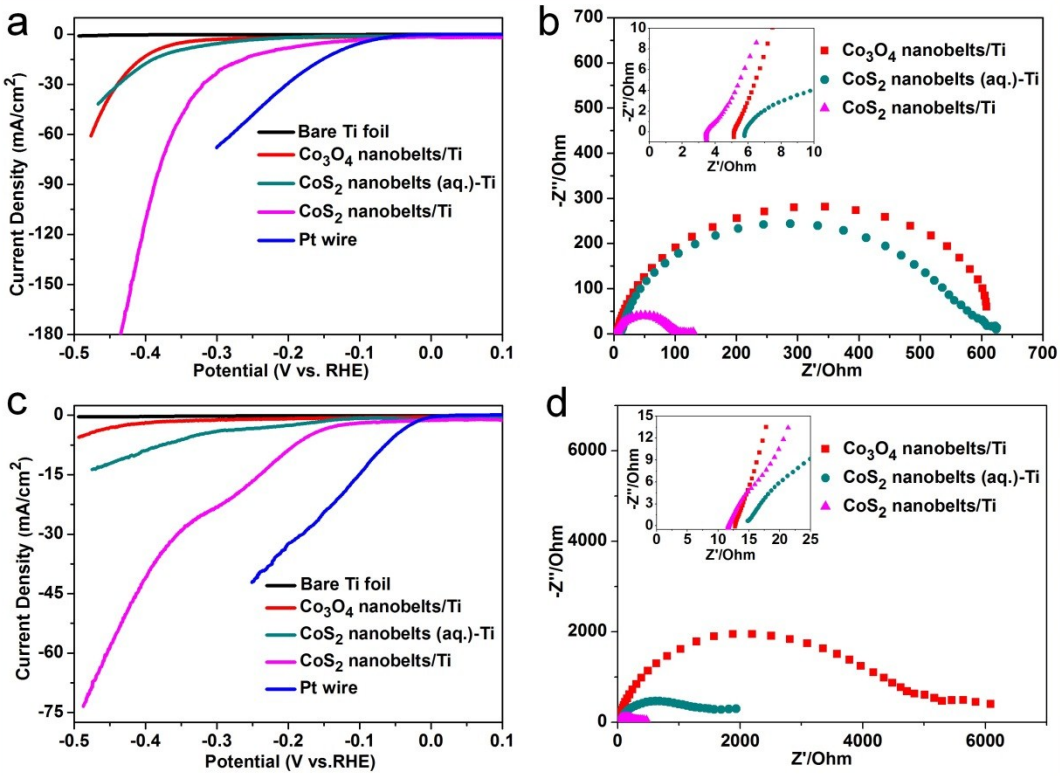

Figure S15. IR-corrected HER polarization curves (a, c) for the Co_3O_4 nanobelts/Ti, CoS_2 nanobelts/Ti, CoS_2 nanobelts(aq.)-Ti and Pt wire, and Nyquist plots (b, d) for the Co_3O_4 nanoelbts/Ti, CoS_2 nanobelts/Ti and CoS_2 nanobelts(aq.)-Ti measured in 1 M KOH electrolyte (a, b) and 1 M PBS (c, d).

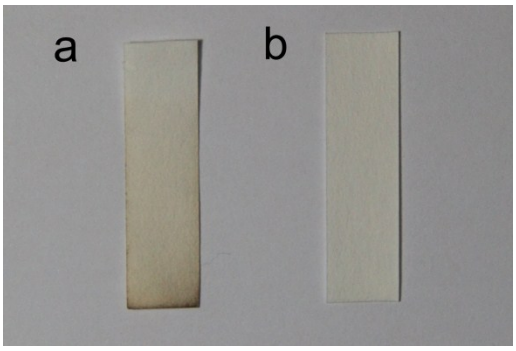

Figure S16. Optical photograph of lead acetate test papers, containing (a) the left one after the first LSV scan and (b) the right one without any test as a blank reference. The possibly occurred reactions list as follows:

$$\text{Cathode}\begin{cases} CoS_2 + 2e^- + 4H^+ \rightarrow Co^{2+} + 2H_2S\uparrow & (1) \\ 2H^+ + 2e^- \rightarrow H_2\uparrow & (2) \end{cases}$$

$$H_2S + Pb(Ac)_2 \rightarrow PbS\downarrow + 2HAc \qquad (3)$$

To probe the corrosion phenomenon during HER process in acid environment, a wettish lead acetate test paper was employed to detect H_2S gas generation and chemical corrosion of catalyst. A short video (Movie S1) is recorded about the first LSV measurement of CoS_2 nanobelts/Ti in 0.5 M H_2SO_4, displaying the gradual color change of a wettish lead acetate test paper from normal white to darker color, accompanied with the release of smelly gas. As well, the corresponding optical photograph (Figure S16) presents obvious color comparison between the darker test paper after the first LSV scan (Figure S16a) and the white one without any test (Figure S16b), both of which derive from the video. As depicted above, we speculate the reduction of S^- ions in CoS_2 to S^{2-} ions and subsequent generation of H_2S gas in acid media (reaction 1) during HER process, which indicates the occurrence of chemical corrosion with several possible reactions listed in Figure S16. Same as cathode reduction reactions (reaction 2), the S^{2-} generation may contribute to the HER current in some degree.

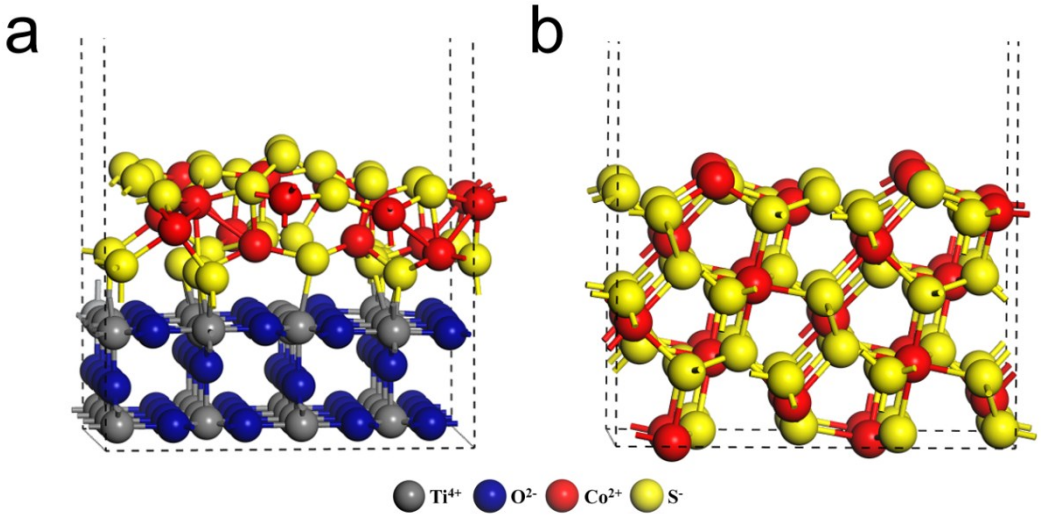

Figure S17. The optimized structures built for transition-state energy calculations before HER started, corresponding to (a) CoS_2 (210)/TiO_2 (110) and (b) CoS_2 (210).

Table S1. The element composition and respective atomic concentration percentage from XPS for both kinds of Ti foil without and after concentrated HCl solution treatment.

Sample	Peak	Atomic conc (%)	Ti:O atom ratio
Bare Ti foil	Ti 2p	19.61	1:2.882
	O 1s	56.52	
	C 1s	23.87	
Bare Ti foil (after HCl treatment)	Ti 2p	25.22	1:1.866
	O 1s	47.07	
	C 1s	27.71	

Table S2. XPS peak values of Co^{3+} $2p_{1/2}$ and $2p_{3/2}$ for $Co(OH)_3$ nanobelts/Ti samples obtained at different reaction times (1 h, 5 h, 20 h), and the peak value differences in Co^{3+} $2p_{1/2}$ and $2p_{3/2}$ between $Co(OH)_3$ nanobelts/Ti samples and normal Co^{3+}-containing sample.

Co^{3+} ($Co(OH)_3$)	Normal[1] (eV)	$Co(OH)_3$ nanobelts/Ti (eV)			Difference (eV)		
		1 h	5 h	20 h	1 h	5 h	20 h
$2p_{1/2}$	801.9	795.2	794.8	797.3	-6.7	-7.1	-4.6
$2p_{3/2}$	785.7	780.3	779.9	781.1	-5.4	-5.8	-4.6

Note: The "normal" refers to unassembled pure phase $Co(OH)_3$ without any heteroatom doped or other phase combined.

Table S3. XPS peak values of Ti^{4+} $2p_{1/2}$ and $2p_{3/2}$ for $Co(OH)_3$ nanobelts/Ti samples obtained at different reaction times (1 h, 5 h, 20 h), and the peak value differences in Ti^{4+} $2p_{1/2}$ and $2p_{3/2}$ between $Co(OH)_3$ nanobelts/Ti samples and bare Ti foil covered with an ultrathin TiO_2 layer.

Ti^{4+} (TiO_2)	Bare Ti foil (eV)	$Co(OH)_3$ nanobelts/Ti (eV)			Difference (eV)		
		1 h	5 h	20 h	1 h	5 h	20 h
$2p_{1/2}$	463.8	463.9	464.1	464.2	0.1	0.3	0.4
$2p_{3/2}$	458.1	458.2	458.5	458.5	0.1	0.4	0.4

Table S4. XPS peak values of O^{2-} 1s for $Co(OH)_3$ nanobelts/Ti samples obtained at different reaction times (1 h, 5 h, 20 h), and the peak value differences in O^{2-} 1s between $Co(OH)_3$ nanobelts/Ti samples and bare Ti foil covered with an ultrathin TiO_2 layer.

O^{2-} (TiO_2)	Bare Ti foil (eV)	$Co(OH)_3$ nanobelts/Ti (eV)			Difference (eV)		
		1 h	5 h	20 h	1 h	5 h	20 h
1s	529.5	529.9	530.0	531.2	0.4	0.5	1.7

Table S5. XPS peak values of Co^{2+} $2p_{1/2}$ and $2p_{3/2}$ for CoS_2 nanobelts/Ti, and the peak value difference in Co^{2+} $2p_{3/2}$ between the CoS_2 nanobelts/Ti sample and normal Co^{2+}-containing sample.

Co^{2+} (CoS_2)	CoS_2 nanobelts (aq.) (eV)	CoS_2 nanobelts/Ti (eV)	Difference (eV)
$2p_{1/2}$	794.1	793.8	-0.3
$2p_{3/2}$	778.9	778.6	-0.3

Note: The "normal" refers to unassembled pure phase CoS_2 without any heteroatom doped or other phase combined. The signal "╳" refers to that the value of Co^{2+} $2p_{1/2}$ for the normal CoS_2 is not available.

Table S6. XPS peak values of Ti^{4+} $2p_{1/2}$ and $2p_{3/2}$ for CoS_2 nanobelts/Ti, and the peak value differences in Ti^{4+} $2p_{1/2}$ and $2p_{3/2}$ between the CoS_2 nanobelts/Ti sample and normal Ti^{4+}-containing sample.

Ti^{4+} (TiO_2)	Normal[3] (eV)	CoS_2 nanobelts/Ti (eV)	Difference (eV)
$2p_{1/2}$	464.0	464.7	0.7
$2p_{3/2}$	458.3	458.6	0.3

Note: The "normal" refers to unassembled pure phase TiO_2 without any heteroatom doped or other phase combined.

Table S7. XPS peak values of S^- $2p_{1/2}$ and $2p_{3/2}$ for CoS_2 nanobelts/Ti, and the peak value difference in S^- $2p_{3/2}$ between the CoS_2 nanobelts/Ti sample and normal S^--containing sample.

S^- (CoS_2)	CoS_2 nanobelts (aq.) (eV)	CoS_2 nanobelts/Ti (eV)	Difference (eV)
$2p_{1/2}$	**163.8**	**163.5**	**-0.3**
$2p_{3/2}$	**162.7**	**162.4**	**-0.3**

Note: The "normal" refers to unassembled pure phase CoS_2 without any heteroatom doped or other phase combined. The signal "╳" refers to that the value of S^- $2p_{1/2}$ for the normal CoS_2 is not available.

Computational Details

All first-principles calculations were carried out using the density-functional theory (DFT), implemented in the CASTEP package. The Perdew–Burke–Ernzerhof (PBE) of the generalized gradient approximation (GGA) was used to describe the exchange and correlation potentials.

For the mulliken charge calculation, the slab model was adopted to simulate the interaction between the rutile TiO_2 (110) surface and nanobelt. To simplify the calculaions, a 2×2 supercell (5.92 Å×12.99 Å) with a surface thickness of ~8.5 Å and a vacuum space of ~12 Å was created. A single stoichiometric $Co(OH)_3$ or CoS_2 cluster was adsorped on the surface, and high coverage was achieved forming an atomic chain along a direction. A plane-wave cutoff energy of 300 eV and the 1×1×1 Monkhorst–Pack k meshes were used. For geometry relaxation, the convergence thresholds for total energy and atomic force components were set at 2×10^{-5} eV and 5×10^{-2} eV/Å, respectively. For the purpose of comparison, the corresponding isolated $Co(OH)_3$ and CoS_2 clusters as well as TiO_2 slab in same unit cell were also calculated.

In order to calculate HER pathway and transition-state energy of H and H_2 groups

on CoS_2 nanobelts/Ti and CoS_2 nanobelts (aq.), the surfaces of CoS_2 (210) and CoS_2 (210)/TiO_2 (110) have been built, as the (210) plane of CoS_2 can match well with the (110) plane of TiO_2. The vacuum space along the z direction is set to be 15 Å, which is enough to avoid interaction between the two neighboring images. Then, H and H_2 groups have been absorbed on the substrate surface. An energy cutoff of 750 eV was used and a k-point sampling set of 5×5×1 were tested to be converged. A force tolerance of 0.01 eV $Å^{-1}$, energy tolerance of 5.0×10^{-7} eV per atom and maximum displacement of 5.0×10^{-4} Å were considered. Each atom in the storage models is allowed to relax to the minimum in the enthalpy without any constraints. The transition state of the whole reactions had been calculated. In addition, the *van der Waals* interactions are available for Grimme scheme (DFT+D).

Adsorption energy E_{ads} of H or H_2 on the substrate was defined as:

$$\Delta E_H = \frac{1}{n}[E(surf + nH) - E(surf) - \frac{n}{2}E(H_2)]$$

where E (surf) and E (surf + nH) denote the energies of bare substrate, H or H_2 being absorbed on substrate. E (H_2) was the energy of H_2 gas and n was the number of H atom.

Free energy change of adsorbed hydrogen of the reaction (ΔG_H) was calculated as:

$$\Delta G_H = \Delta E_H + \Delta ZPE - T\Delta S$$

where ΔE_H is the calculated adsorption energy difference of H species, and ΔZPE and ΔS are the energy differences of zero point energy and entropy between the initial and final states, respectively. The value of (ΔZPE-TΔS) is 0.28 eV, just as "$\Delta G_H = \Delta E_H$ + 0.28 eV". Additionally, the hydrogen coverage of 1/16 S atoms is adopted for corresponding calculations and the free energy of "$H^+ + e^-$" is defined equal to that of 1/2 H_2 under standard conditions (1 bar of H_2 and pH= 0 at 300K).

Table S8. Mulliken population analysis of the typical $Co(OH)_3$ nanobelts/Ti from DFT calculations.

Ions	Mulliken charge		
	$Co(OH)_3$ or TiO_2 (*e*)	$Co(OH)_3$ /TiO_2 (*e*)	Variation (*e*)
Co^{3+}	+0.93	+0.56	-0.37
Ti^{4+} (1)	+1.01	+1.13	0.12
Ti^{4+} (2)	+0.98	+1.15	0.17
Ti^{4+} (3)	+0.85	+0.94	0.09
O^{2-} (1)	-0.81	-0.80	0.01
O^{2-} (2)	-0.80	-0.77	0.03
O^{2-} (3)	-0.84	-0.83	0.01
O^{2-} (4)	-0.65	-0.62	0.03

Table S9. Mulliken population analysis of the CoS_2 nanobelts/Ti from DFT calculations.

Ions	Mulliken charge		
	CoS_2 or TiO_2 (*e*)	CoS_2 /TiO_2 (*e*)	Variation (*e*)
Co^{2+}	+0.41	+0.24	-0.17
Ti^{4+} (1)	+1.30	+1.18	-0.12
Ti^{4+} (2)	+1.30	+1.18	-0.12
Ti^{4+} (3)	+1.27	+1.29	0.02
Ti^{4+} (4)	+1.26	+1.30	0.04
Ti^{4+} (5)	+1.27	+1.29	0.02
Ti^{4+} (6)	+1.27	+1.29	0.02
Ti^{4+} (7)	+1.26	+1.30	0.04
Ti^{4+} (8)	+1.27	+1.29	0.02
S^{-} (1)	-0.21	-0.23	-0.02
S^{-} (2)	-0.21	-0.23	-0.02

Table S10. Bond population analysis of the CoS_2 nanobelts/Ti from DFT calculations.

Bond	Bond population (e)
Ti^{4+} (1)-S^{-} (1)	0.51
Ti^{4+} (2)-S^{-} (2)	0.51
Ti^{4+} (1)-O^{2-} (1)	0.40
Ti^{4+} (1)-O^{2-} (2)	0.40
Ti^{4+} (1)-O^{2-} (4)	0.40
Ti^{4+} (1)-O^{2-} (5)	0.40
Ti^{4+} (1)-O^{2-} (7)	0.38
Ti^{4+} (2)-O^{2-} (2)	0.40
Ti^{4+} (2)-O^{2-} (3)	0.40
Ti^{4+} (2)-O^{2-} (5)	0.40
Ti^{4+} (2)-O^{2-} (6)	0.40
Ti^{4+} (2)-O^{2-} (8)	0.38
Ti^{4+} (4)-O^{2-} (9)	0.45
Ti^{4+} (6)-O^{2-} (10)	0.45
Ti^{4+} (9)-O^{2-} (11)	0.44
Ti^{4+} (10)-O^{2-} (13)	0.44
Ti^{4+} (8)-O^{2-} (6)	0.38
Ti^{4+} (7)-O^{2-} (5)	0.36
Ti^{4+} (12)-O^{2-} (13)	0.39
Ti^{4+} (11)-O^{2-} (11)	0.39
Ti^{4+} (11)-O^{2-} (12)	0.39

References:

1. J. Yang, H. Hyodo, K. Kimura and T. Sasaki, *Nanotechnology*, 2010, **21**, 045605.
2. S. Deng, N. Chen, D. Deng, Y. Li, X. Xing and Y. Wang, *Ceram. Int.*, 2015, **41**, 11004-11012.
3. Q. G. Zeng, Z. J. Ding and Z. M. Zhang, *J. Lumin.*, 2006, **118**, 301-307.